ELSEVIER

Journal of Nuclear Materials 241–243 (1997) 941–945

journal of nuclear materials

A 2D approach to island divertor modelling for Wendelstein 7-AS

G. Herre [a,*], R. Schneider [a], D. Coster [a], F. Sardei [a], D. Reiter [a,b], P. Grigull [a], J. Kisslinger [a]

[a] *Max-Planck-Institut für Plasmaphysik, EURATOM Association, Boltzmannstr. 2, D-85748 Garching, Germany*
[b] *Forschungszentrum Jülich GmbH, EURATOM Association, D-52425 Jülich, Germany*

Abstract

The properties of an island divertor for Wendelstein 7-AS were investigated by using the B2-Eirene package. Because B2 is a two dimensional code the calculation needs to be done on a toroidally averaged grid. Carbon influx resulting from physical and chemical sputtering was treated self-consistently. The model predicts a transition from low to high recycling at a separatrix density of $1 * 10^{19}$ m^{-3}. A detailed discussion of the momentum removal mechanism for this geometry will be presented.

Keywords: W7-AS; Stellarator; 2D model; Helical divertor

1. Introduction

The finite aspect ratio of a real stellarator leads to toroidal coupling between magnetic field components of different spatial symmetry. This toroidal coupling causes generally a destruction of the outer magnetic surfaces. Depending on the strength of the field components a chain of natural islands may emerge at resonant surfaces (resonance between the symmetry of the field component and the rotational transform). These natural islands can be used for divertor operation. The primary goals of a divertor are: to allow parallel energy losses to reduce the power load on the target plates, screening of the main plasma from impurities and provide high neutral gas density in front of the target plates to enable efficient pumping. To study the possibility of using the natural islands of W7-AS as a divertor configuration, a 2D-multi-fluid code (B2) coupled with a 3D-Monte-Carlo neutral gas code (Eirene) was applied. In B2-Eirene practically all atomic physics relevant for describing edge plasma phenomena is incorporated. Therefore it can be used to determine leading parameters for an island divertor. Because B2 is a two dimensional code the calculation needs to be done on a toroidally averaged grid (Section 2). In Section 3 the main aspects of the B2-Eirene package related to this work will be introduced. The choices of the free parameters and boundary conditions will be explained in Section 4. Mainly, two different sets of density scans have been made, one pure deuterium density scan and a multi-fluid scan (deuterium plus carbon) where carbon comes from physical and chemical sputtering from the target plates. In Section 5 results from these calculations will be presented.

2. Grid generation for W7-AS

W7-AS is a modular stellarator with $n = 5$ magnetic field periods. The value of the rotational transform $\iota/2\pi$ can be chosen within the range of $0.2 < \iota/2\pi < 0.7$. With increasing rotational transform the magnetic separatrix shrinks so that at the present limiter configuration, divertor action may be expected for values of $\iota/2\pi > 0.4$. For this study a configuration with an edge rotational transform close to 5/9 was chosen. In this case nine connected islands appear outside the main plasma, as can be seen on the Poincaré-plot shown in Fig. 1. At present, ten symmetrically placed inboard limiters are installed in W7-AS that may be seen as target plates in this configuration. Using

* Corresponding author. Fax: +49-89 3299 2584; e-mail: herre@ipp.mpg.de.

PII S0022-3115(96)00636-8

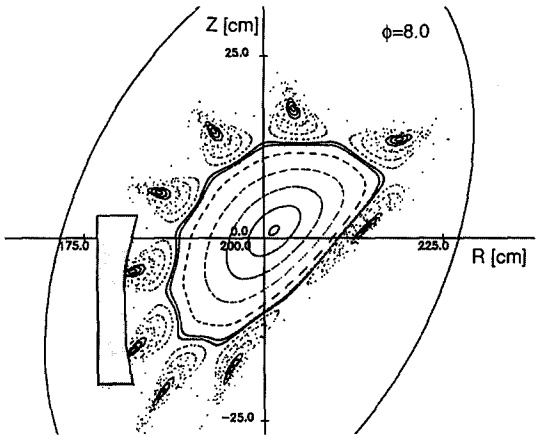

Fig. 1. Poincaré-plot of W7-AS for an edge rotational transform $\iota_a/2\pi = 0.564$. The inboard limiter is shown shaded on the lower-left part of the figure.

three different sets of Fourier coefficients for the inner, island and outer part of the plasma a three dimensional grid was constructed and made as orthogonal as possible. The geometry coefficients needed for the B2-calculation were averaged (distances) or summed up (areas, volumes) toroidally along the whole island. An averaged grid used for the neutral gas calculation shown in Fig. 2 was also constructed. The calculated region extends about 4 cm into the core region to cover the whole region where atomic processes involving neutrals are important.

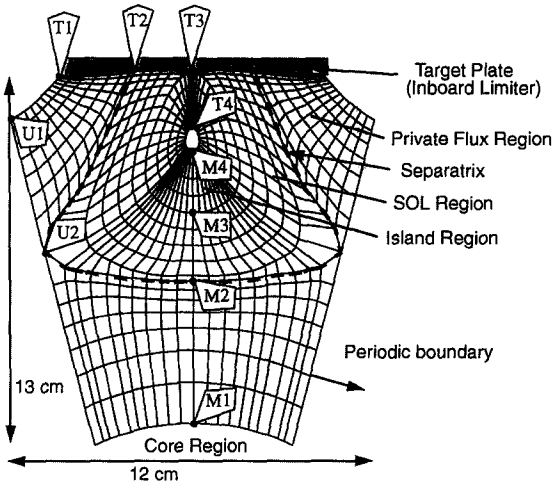

Fig. 2. Geometrical grid resulting from toroidally averaging along one island. Radial profiles from point M1 to M4 are called midplane profiles. Profiles along the points T1, T2, T3 and T4 are called target plate profiles. Notice that the part from T3 to T4 lies within the closed island.

3. B2-Eirene package

The B2(Braams)-code [1] solves the continuity, parallel momentum and energy equations. Parallel transport is described by Navier–Stokes type equations. For radial transport an anomalous diffusive Ansatz is made. The special topology in our case, see Fig. 2, is treated by three cuts in the numerical grid. Two cuts are needed to treat the periodic boundary condition at the connection to the neighbouring island. The third cut provides a connection of the grid cells in the closed island (line from T3 to T4 in Fig. 2). This cut technique originally developed for single-null tokamak divertor cases, where only two cuts are needed, could be straightforwardly extended to our special topology. For the parallel transport coefficients the classical values are used. The Eirene-code [2] calculates from a given plasma state, via a Monte-Carlo technique, the neutral gas distribution and source terms for the B2 fluid model. Also physical and chemical sputtering is treated by Eirene to yield the carbon sources for the multi-fluid calculations. In that case the full 21-momentum approach is used [3]. All the calculations made in this study have been done by using the coupled B2-Eirene [4–7] package which also allows time-dependent calculations, however here we are only interested in stationary solutions.

4. Free parameters and boundary conditions

The radial transport coefficients are assumed to be anomalous and their values have to be determined by comparison with experimental data. The radial diffusion coefficient was chosen according to the scaling law given in Ref. [8] which gives 0.5 m^2/s for the higher density cases. For most calculations the same value (0.5 m^2/s) was used for the radial viscosity and diffusion coefficient. This is justified by the assumption that turbulence is the reason for anomalous transport of both particles and momentum and this turbulence is approximately perpendicular to the magnetic field. Both values (radial viscosity and diffusion coefficient) were also varied in sensitivity studies. For carbon the same values as for deuterium were assumed. No pinch velocity was used for deuterium or carbon. Anomalous heat conduction for electrons was taken three times the particle diffusion coefficient (1.5 m^2/s) and 1.0 m^2/s for the ions. At the innermost flux surface of the grid the total power outflux from the core, deuterium density and zero net flux for all carbon ions was prescribed. This zero flux condition does not allow for the diffusion of lower charged carbon states into the core plasma, getting ionised and diffusing back into the calculation region. This results in a non-reliable CVI–CVII ratio close to the core plasma but should have only a minor affect on the lower ionised carbon states in the SOL or island region. The total power flux from the core plasma was set to 220 kW for the pure deuterium case (radiative losses in the core and edge plasma were taken into ac-

count) and 500 kW for the multi-fluid case (radiative losses from the core were taken into account). The density was varied between $5*10^{18}$–$5*10^{19}$ m^{-3}. At the target plates, sheath boundary conditions were used for all equations. Towards the private flux region, radial decay lengths (2 cm for densities and 3 cm for temperatures) have been fixed. At the center of the closed island (O-point) no net radial flux of particles, momentum or energy was assumed. Periodic boundary conditions have been used at the connection to the neighbouring island.

5. Results

The pure deuterium density scan shows a transition from low to high recycling at a separatrix density of about $1*10^{19}$ m^{-3}. Radial density, electron temperature and pressure profiles at the midplane and along the target plate for two different densities are shown in Figs. 3–5. The lower density case (circles in Fig. 3) is a medium recycling case where the density drops along the separatrix from $7*10^{18}$ m^{-3} to $4.5*10^{19}$ m^{-3} at the target plate. In the case of a separatrix density of $1.3*10^{19}$ m^{-3} a high recycling regime characterised by an enhanced density at the target plate (black triangles Fig. 3) compared to the midplane (open triangles) is found in the SOL. The calculated temperatures in front of the target plates are 50/25 eV (electron/ion) for the medium recycling case and 20/15 eV for the high recycling case. In both cases a strong radial dependence of the parallel pressure drop between the stagnation point and the target plate was found. The pressure drop varies from about 5 at the separatrix to about 2 just outside the closed island. Analysing the parallel momentum balance, keeping only the important terms for the cases just shown the pressure

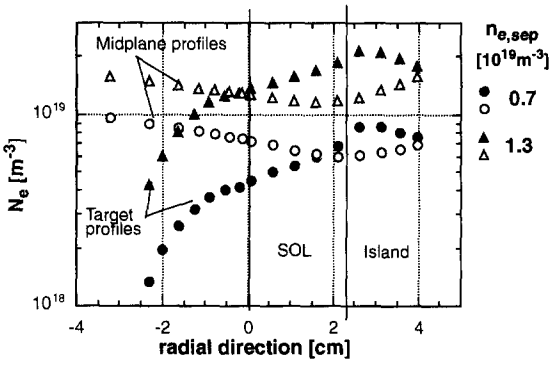

Fig. 3. Radial density profiles at the midplane (open symbols) and along the target plate (full symbols) for a medium recycling and a high recycling case. The position of the profiles shown is explained in Fig. 2. The abscissa is centered at the separatrix position (point M2, T2 in Fig. 2), positive values are directed towards the center of the island. The points with abscissa values > 2.5 cm are located within the closed island region.

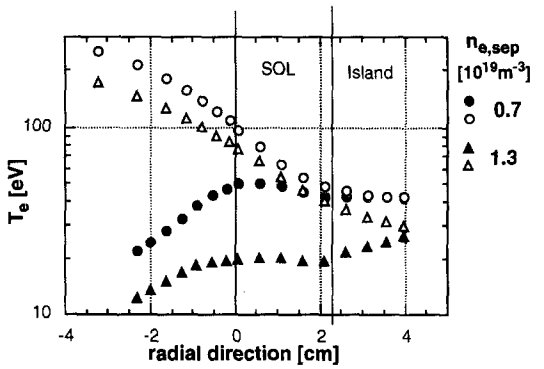

Fig. 4. Same as Fig. 3 except that the electron temperature is shown.

balance reads with: m ion mass, n density, u parallel velocity, v radial velocity, p total pressure, $\eta_\perp$ radial viscosity, S_m momentum source from neutral gas calculation, x parallel-, r radial coordinate:

$$\frac{\partial}{\partial x}(mnu^2+p)+\frac{\partial}{\partial r}\left(mnuv-\eta_\perp\frac{\partial u}{\partial r}\right)=S_m. \quad (1)$$

Without any momentum loss, a pressure drop by a factor of 2 results only from the acceleration to sound velocity at the entrance to the sheath of the target plate. To discriminate between convection and viscous momentum transfer the radial viscosity was reduced by a factor of 100 to 0.005 m^2/s. This reduction leads to a reduced pressure drop (about 4 at the separatrix) and an increased density enhancement in front of the target plates from 1.3 ($\eta_\perp$ = 0.5 m^2/s) to 1.9 ($\eta_\perp = 0.005$ m^2/s). The momentum transfer can be seen from the radial profiles of the ram pressure (ratio of target plate/upstream sum of static and dynamic pressure) shown in Fig. 6. For both values of $\eta_\perp$ we see an outward transport of momentum indicated by a momentum sink in the SOL (ram pr. < 1) and a momentum source in the private flux region (ram pr. > 1). The higher viscosity (open circles in Fig. 6) leads to a radially broader distribution of the momentum sources. In this case

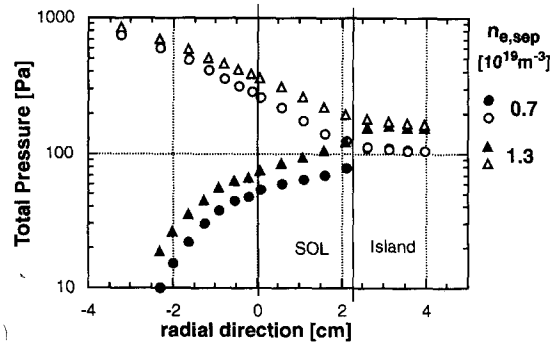

Fig. 5. Same as Fig. 3 except that the total pressure is shown.

($\eta_\perp = 0.5$ m^2/s) the momentum losses from the Eirene calculation contribute less than 10% to the pressure loss in the SOL. For the $\eta_\perp = 0.005$ m^2/s case the convective loss of momentum and loss due to neutrals are of the same size. The total integral pressure drop is about 10% for $\eta_\perp = 0.005$ m^2/s and 20% for $\eta_\perp = 0.5$ m^2/s with the following definition:

$$1 - \left(\int_{\text{along target}} p^* \, \mathrm{d}\Psi \Big/ \int_{\text{upstream}} p^* \, \mathrm{d}\Psi \right), \qquad (2)$$

where Ψ is the magnetic flux, and p^* and the path of integration is explained in caption of Fig. 6. Because the overall radial behaviour of the ram pressure in Fig. 6 is nearly independent of $\eta_\perp$ we conclude that the radial momentum transport is mainly due to convective flux (see Eq. (1)), which itself is driven by the strong gradients at the separatrix. Normally the value for the poloidal diffusion was chosen equal to the radial diffusion coefficient. A control calculation without poloidal diffusion gave high poloidal density gradients (factor 10 larger than radial gradient) at the outer stagnation point (line between T3 and T4 in Fig. 2) which seems unrealistically high to us because of the strong turbulence in the SOL. That means poloidal diffusion must be considered in this geometry. The relative ratio between the strength of the parallel and cross-field transport depends on the field line pitch, which is in our case extremely small: $B_\theta/B \approx 0.001$–0.003 in the SOL. To be able to study this dependence of the field line pitch not only numerically, control coils will be installed at W7-AS, that enable modifications of the island rotational transform and size. The experimental transition from low to high recycling was found at a factor 3 higher separatrix density [9]. Reasons for finding a lower onset to high-recycling with this model may be caused by the 2D approximation which neglects the effect of the toroidally inhomogeneous plasma parameters, neutral gas and impurity distribution. Because of the problem measuring the total radiation level in our 3D-geometry the input power used in the calculation may differ from the one experimental available and this could explain the higher onset of the high-recycling regime.

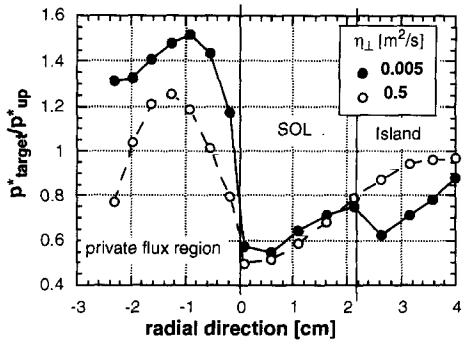

Fig. 6. Radial profile of the ratio $p^*_{\text{target}} / p^*_{\text{up}}$, where $p^* = p(1 + \gamma M^2)$, p total pressure, γ adiabatic coefficient, M mach number. p^*_{target} goes from T1 to T4 (Fig. 2) and p^*_{up} is taken along the line U1-U2-M4.

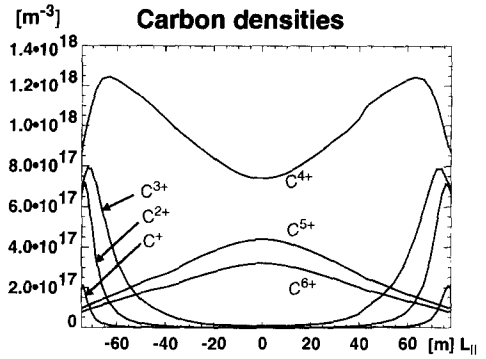

Fig. 7. Radially integrated (along the SOL-layer) parallel carbon density profiles. The partly overlapping C^+, C^{2+} and C^{3+} layers can be seen.

The multi-fluid calculations also predict high recycling at separatrix densities larger than $1 * 10^{19}$ m^{-3}. For a separatrix density of $1.2 * 10^{19}$ m^{-3}, a target density of $2.1 * 10^{19}$ m^{-3} and electron(ion) temperatures of 18(18) eV are predicted. The total radiation level in this case was about 50% which is comparable to experimental data. Because the radiation layer is located within one cm in front of the target plates about half of the radiated power is also absorbed by the target plate, that only a power load reduction of about 25% is expected. About half of the power arriving at the target plate comes from the private zone. To get higher power load reductions a detached plasma state is necessary. Studies on the existence and the stability of a detached plasma in this geometry are under way. Clear shell structures for the different carbon species could be found (Fig. 7). The CII-CIV layers are located just in front of the target, whereas CV is spread out through the whole SOL and island region. These results agree qualitatively with experimental results and may be used for quantitative verification via spectroscopic measurements.

6. Conclusion

B2-Eirene code was successfully used to model edge plasma behaviour on a toroidally averaged grid for W7-AS. Because of the small field line pitch cross-field transport plays an important role for the edge plasma parameters. High recycling with a density enhancement of about 1.5 and low temperatures in front of the target plates can be achieved in this configuration. In this case a parallel pressure drop of a factor of 5 was found at the separatrix which is balanced by convective radial momentum transport. Radial viscosity makes only small contributions to

the momentum balance but still changes the plasma parameters close to the target plates up to 50%. To enable detailed profile comparison with experimental data for model-validation a full 3D-approach is necessary as it is explained in more detail in Refs. [10,11].

References

[1] B.J. Braams, A Multi Fluid Code for Simulation of the Edge Plasma in Tokamaks, Report No. (NET) EUR-FU/XII-80/87/68, Comm. of the EC, Brussels (1987).
[2] D. Reiter, The EIRENE Code, Version: Jan. 92, Users Manual, Report No. 2599, Institut für Plasmaphysik, Association EURATOM-KFA (1992).
[3] A. Bergmann, Yu. Igitkhanov et al., Contrib. Plasma Phys. 36(2–3) (1996) 192–196.
[4] D. Reiter, J. Nucl. Mater. 196–198 (1992) 80–89.
[5] R. Schneider, D. Reiter, H.-R Zehrfeld, B. Braams, M. Baelmans, J. Geiger, H. Kastelewicz, J. Neuhauser and R. Wunderlich, J. Nucl. Mater. 196–198 (1992) 810–815.
[6] R. Schneider, B. Braams, D. Reiter, H.-R Zehrfeld, J. Neuhauser, M. Baelmans, H. Kastelewicz and R. Wunderlich, Contrib. Plasma Phys. 32(3–4) (1992) 450–455.
[7] D. Reiter et al., J. Nucl. Mater. 220–222 (1995).
[8] P. Grigull et al., Edge transport studies on the W7-AS stellarator, 10th Int. Conf. on Stellarators, IAEA Technical Meeting, Madrid, Spain, 1995, Report EUR-CIEMAT, Vol. 30 (1995) p. 73.
[9] P. Grigull et al., these Proceedings, p. 935.
[10] Y. Feng et al., these Proceedings, p. 930.
[11] F. Sardei et al., these Proceedings, p. 135.